The $\alpha_2\delta$-1 subunit remodels $Ca_V1.2$ voltage sensors and allows Ca^{2+} influx at physiological membrane potentials

Nicoletta Savalli,[1] Antonios Pantazis,[1] Daniel Sigg,[5] James N. Weiss,[2,3,4] Alan Neely,[1,6] and Riccardo Olcese[1,3,4]

[1]Department of Anesthesiology, Division of Molecular Medicine, [2]Department of Medicine (Cardiology), [3]Department of Physiology, and [4]Cardiovascular Research Laboratories, David Geffen School of Medicine, University of California, Los Angeles, Los Angeles, CA 90095

[5]dPET, Spokane, WA 99223

[6]Centro Interdisciplinario de Neurociencias de Valparaíso, Facultad de Ciencias, Universidad de Valparaíso, Valparaíso 2360102, Chile

Excitation-evoked calcium influx across cellular membranes is strictly controlled by voltage-gated calcium channels (Ca_V), which possess four distinct voltage-sensing domains (VSDs) that direct the opening of a central pore. The energetic interactions between the VSDs and the pore are critical for tuning the channel's voltage dependence. The accessory $\alpha_2\delta$-1 subunit is known to facilitate $Ca_V1.2$ voltage-dependent activation, but the underlying mechanism is unknown. In this study, using voltage clamp fluorometry, we track the activation of the four individual VSDs in a human L-type $Ca_V1.2$ channel consisting of α_{1C} and β_3 subunits. We find that, without $\alpha_2\delta$-1, the channel complex displays a right-shifted voltage dependence such that currents mainly develop at nonphysiological membrane potentials because of very weak VSD–pore interactions. The presence of $\alpha_2\delta$-1 facilitates channel activation by increasing the voltage sensitivity (i.e., the effective charge) of VSDs I–III. Moreover, the $\alpha_2\delta$-1 subunit also makes VSDs I–III more efficient at opening the channel by increasing the coupling energy between VSDs II and III and the pore, thus allowing Ca influx within the range of physiological membrane potentials.

The Journal of General Physiology

INTRODUCTION

Calcium influx through voltage-activated calcium (Ca_V) channels translates electrical signals into a variety of physiological outcomes such as cell contraction, neurotransmitter or hormonal release, and gene expression (Catterall, 2011; Zamponi et al., 2015). The specificity of the Ca^{2+} signal relies on the activity of the Ca_V channel complex being perfectly tuned to voltage signals. Ca_V channels are multimeric proteins formed by the pore-forming α_1 subunit and at least three auxiliary subunits, β, $\alpha_2\delta$, and calmodulin, in a 1:1:1:1 stoichiometry, resulting in an asymmetric structural architecture (Fig. 1; Findeisen and Minor, 2010; Catterall, 2011; Dolphin, 2013; Ben-Johny and Yue, 2014; Neely and Hidalgo, 2014; Campiglio and Flucher, 2015; Wu et al., 2015). The $\alpha_2\delta$ auxiliary subunit is a large (~170 kD), mostly extracellular protein with a single membrane-anchoring segment (Davies et al., 2010) that binds to the α_1 subunit from the extracellular side (Cassidy et al., 2014). α_2 and δ proteins are the products of the same gene as a preprotein that is posttranslationally proteolysed and then linked by a disulfide-bond to form the mature $\alpha_2\delta$ protein (Calderón-Rivera et al., 2012). Four genes (CACNA2D1–4) encode for distinct $\alpha_2\delta$ isoforms ($\alpha_2\delta$-1–4), which are all expressed in the brain (Dolphin, 2013). In addition to brain tissue, $\alpha_2\delta$-1 is strongly expressed in cardiac, smooth, and skeletal muscles, whereas $\alpha_2\delta$-4 is found in endocrine tissues and the retina. Mutations in the $\alpha_2\delta$-1 gene can lead to Brugada (Burashnikov et al., 2010) and short QT (Templin et al., 2011; Bourdin et al., 2015) syndromes and are associated with epilepsy and mental disability (Vergult et al., 2015). In mice, naturally occurring mutations in the $\alpha_2\delta$-2 gene lead to ataxia and epilepsy (Barclay et al., 2001), whereas the $\alpha_2\delta$-3 protein is important for synaptic morphogenesis (Kurshan et al., 2009) and nociception (Neely et al., 2010). Mutations in $\alpha_2\delta$-4 can result in night blindness (Wycisk et al., 2006). Moreover, $\alpha_2\delta$-1 and -2 have been identified as the molecular targets of gabapentinoid drugs (such as gabapentin and pregabalin), mediating their analgesic action in neuropathic pain (Field et al., 2006; Hendrich et al., 2008; Uchitel et al., 2010). Finally, it has been shown that $\alpha_2\delta$ proteins also play an important role in synapse formation (Eroglu et al., 2009).

Several studies report that the interaction of $\alpha_2\delta$-1 with the pore-forming α_{1C} subunits (L-type $Ca_V1.2$) favors channel activation, as manifested by a hyperpolar-

Correspondence to Riccardo Olcese: rolcese@ucla.edu

Abbreviations used: cryo-EM, cryo-electron microscopy; MES, methanesulfonate; VCF, voltage clamp fluorometry; VSD, voltage-sensing domain.

The Rockefeller University Press $30.00
J. Gen. Physiol. 2016 Vol. 148 No. 2 147–159
www.jgp.org/cgi/doi/10.1085/jgp.201611586

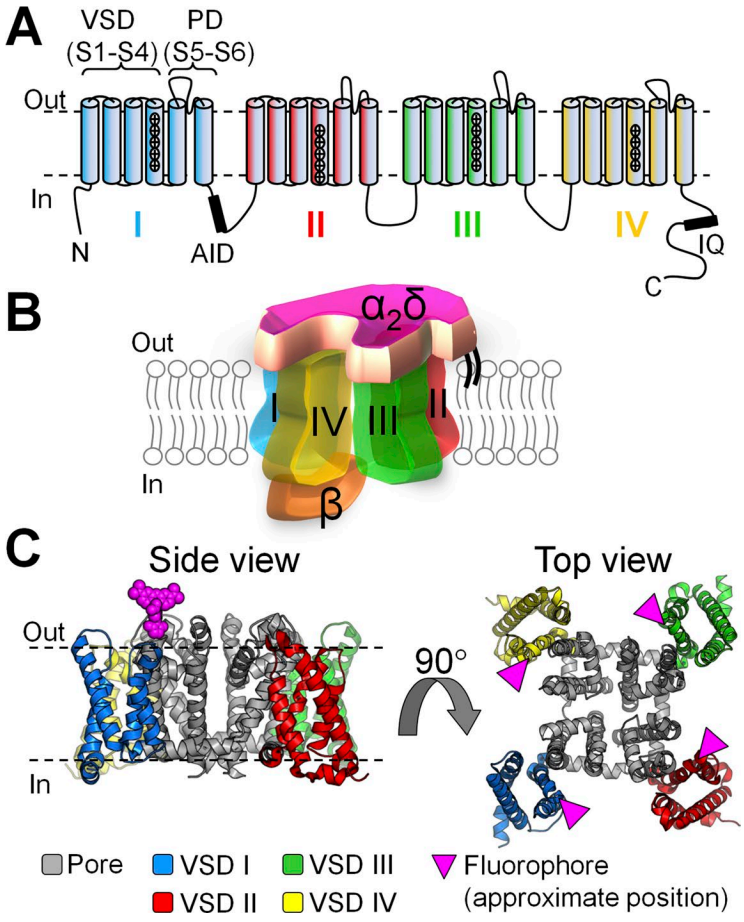

Figure 1. **$Ca_V1.2$ channel topology and subunit composition.** (A) In $Ca_V1.2$, the pore-forming α_{1C} subunit consists of four tandem repeats (I–IV), each crossing the membrane six times (S1–S6). Helices S1–S4 form the VSD, and helices S5 and S6 form the pore domain (PD). The intracellular loop between repeats I and II encompasses the binding site for the auxiliary β subunit (α-interacting domain [AID]), whereas the C terminus includes the IQ region, where calmodulin binds. (B) $Ca_V1.2$ channels are multimeric proteins composed of the α_{1C} pore-forming subunit, a mostly extracellular $\alpha_2\delta$ subunit, and an intracellular β subunit. In this cartoon representation, the four repeats that constitute the α_{1C} subunit are arranged clockwise, as in a recent cryo-EM structure of related α_{1S} ($Ca_V1.1$) channel (Wu et al., 2015): repeats III (green) and IV (yellow) are in the front, whereas I (blue) and II (red) are in the back. (C) Side and top views of the atomic structure of a voltage-gated Na^+ channel (Na_VAb; PDB accession no. 4EKW; Payandeh et al., 2012), shown as putative structural representation of a Ca_V α_1 channel. S4 helices were fluorescently labeled at their extracellular flank, one VSD at a time (pink triangles).

izing shift of channel opening (Felix et al., 1997; Platano et al., 2000; Bourdin et al., 2015) and an accelerated time course of activation (Bangalore et al., 1996). Accordingly, channel activation is diminished with $\alpha_2\delta$-1 down-regulation (Tuluc et al., 2007; Fuller-Bicer et al., 2009) and enhanced with $\alpha_2\delta$-1 up-regulation (Li et al., 2006). Thus, by facilitating channel opening, $\alpha_2\delta$-1 allows $Ca_V1.2$ channels to operate at physiological membrane potentials. However, the molecular mechanism by which $\alpha_2\delta$-1 facilitates $Ca_V1.2$ activation is as yet poorly understood.

Because $\alpha_2\delta$-1 modulates the voltage-dependent properties of $Ca_V1.2$ channels (Felix et al., 1997; Platano et al., 2000; Bourdin et al., 2015) and associates with α_{1C} subunits asymmetrically (Walsh et al., 2009a), we hypothesized that $\alpha_2\delta$-1 differentially modulates each of the four voltage-sensing domains (VSDs), as well as their contribution to channel opening. In fact, the pore-forming α_{1C} subunit consists of four homologous, but nonidentical, concatenated repeats (I–IV), each composed of a VSD (transmembrane helices S1–S4) and a quarter of the pore domain (S5–S6; Catterall, 2011). Using voltage clamp fluorometry (VCF), we have recently revealed the functional heterogeneity of the four $Ca_V1.2$ VSDs, whereby each undergoes structural changes during channel activation, with unique voltage- and time-dependent properties, such that the activation of VSDs II and III, and to a lesser extent VSD I, energetically contributes to channel opening (Pantazis et al., 2014). VCF is a powerful investigative tool that allows for simultaneous measurements of ionic current kinetics and structural rearrangements occurring within specific protein domains, the latter tracked using environmentally sensitive fluorophores (Claydon and Fedida, 2007; Gandhi and Olcese, 2008; Talwar and Lynch, 2015; Zhu et al., 2016). VCF has been a successful approach in the study of numerous voltage-sensitive proteins (Mannuzzu et al., 1996; Cha et al., 1999; Smith and Yellen, 2002; Savalli et al., 2006; Kohout et al., 2008; Osteen et al., 2010; Tombola et al., 2010), transporters (Meinild et al., 2002; Larsson et al., 2004; Ghezzi et al., 2009), and receptors (Dahan et al., 2004; Lörinczi et al., 2012). Using VCF, auxiliary subunit modulation of VSDs has also been detected in ion channels, such as BK channels (Savalli et al., 2007) or $K_V7.1$ (Ruscic et al., 2013). However, VCF has only recently been adapted to investigate Ca_V channels (Pantazis et al., 2014).

In this study, by using VCF and a structurally relevant allosteric model of $Ca_V1.2$ activation, we show that the $\alpha_2\delta$-1 auxiliary subunit (a) facilitates the voltage-dependent activation of $Ca_V1.2$ VSDs I–III; (b) accelerates VSD I kinetics; and (c) increases the energetic contribu-

tion of VSDs I–III to pore opening. These results unravel the molecular mechanisms by which $\alpha_2\delta$-1 exerts its modulation on $Ca_V1.2$ channel activation, allowing for Ca^{2+} influx to occur in excitable cells at physiological membrane potentials.

MATERIALS AND METHODS

Molecular biology

Human $\alpha_{1C\text{-}77}$ subunits (GenBank accession no. CAA84346; Soldatov, 1992) of $Ca_V1.2$ channels, with a Cys substituted at an extracellular position in the S3–S4 linker of each VSD at a time, were used (F231C, L614C, V994C, or S1324C for VSDs I–IV, respectively) as previously described (Pantazis et al., 2014). Single-point mutations were generated using the QuikChange Site-Directed Mutagenesis kit (Agilent Technologies) and confirmed by sequencing. Auxiliary subunits $\alpha_2\delta$-1 (UniProt accession no. P13806) and β_3 (UniProt accession no. P54286) were also coexpressed. The cRNA of the different subunits was transcribed in vitro (mMES SAGE MACHINE; Ambion) and injected into stage VI *Xenopus laevis* oocytes (50 nl at 0.1–0.5 µg/µl).

VCF

3–4 d after injection, oocytes were incubated with thiol-reactive fluorophores sensitive to environmental changes (10 µM tetramethylrhodamine-5-maleimide [TMRM] for VSD II and 20 µM 2-((5(6)-tetramethyl-rhodamine)carboxylamino)ethyl methanethiosulfonate [MTS-TAMRA] for VSD I, III, or IV) in a depolarizing solution (120 mM K-methanesulfonate [MES], 2 mM $Ca(MES)_2$, and 10 mM HEPES, pH 7.0). Subsequently, oocytes were voltage clamped using the cut-open oocyte technique (Stefani and Bezanilla, 1998; Pantazis and Olcese, 2013). Fluorescence changes and ionic currents were acquired simultaneously from the same membrane area (Gandhi and Olcese, 2008; Pantazis and Olcese, 2013). External solution was 2 mM $Ba(MES)_2$, 120 mM NaMES, and 10 HEPES, pH 7.0, supplemented with 0.1 ouabain to eliminate charge movement from Na/K ATPase (Neely et al., 1994). Internal solution was 120 mM K-glutamate and 10 mM HEPES, pH 7.0. Pipette solution was 2.7 M Na-MES, 10 mM NaCl, and 10 mM Na-HEPES, pH 7.0. Before experiments, oocytes were injected with 10 mM BAP TA•4K, pH 7.0, to prevent activation of native Ca^{2+}- and Ba^{2+}-dependent Cl^- channels (Barish, 1983).

Data analysis

The voltage dependence of ionic conductance (G(V), estimated from the peaks of the tail currents) and fluorescence changes (F(V)) were empirically characterized by fitting to one or two Boltzmann functions as $f(V) = \{1 + \exp([q \cdot (V_{half} - V_m)(F/RT)])\}^{-1}$, where q is the effective charge, V_{half} is the half-activation potential, V_m is the membrane potential, T is the absolute temperature, and F and R are the Faraday and Gas constants, respectively. F(V) curves can be satisfactorily described by single Boltzmann functions both the absence and the presence of the $\alpha_2\delta$-1 subunit (see Figs. 4 and 5).

The time course of fluorescence onset (VSD activation) was fitted in background-subtracted fluorescence traces to the sum of two exponential components:

$$f(t) = B + \sum_{i=1}^{2} A_i \cdot \exp(-t/\tau_i),$$

where B is the baseline, A is the amplitude, t is time, and τ is the time constant. Fitting was performed in Matlab (MathWorks) by least squares (Optimization Toolbox). Only traces with sufficient signal-to-noise ratio (S:N >2) were included in the kinetics statistics. S:N is defined as mean signal amplitude divided by the root mean square. Fractional amplitude–weighted time constants (τ_{avg}) were calculated using

$$\tau_{avg} = \sum_{i=1}^{2} \alpha_i \cdot \tau_i,$$

where

$$\alpha_i = \frac{A_i}{A_1 + A_2}.$$

Data are reported as mean ± SEM; statistical analysis was performed using Excel (Microsoft).

Allosteric model

Modeling $Ca_V1.2$ kinetics and activation curves through a five-particle allosteric scheme was performed as described previously (Pantazis et al., 2014).In brief, equilibrium states were determined from the values of five particle equilibrium constants (L, $J_{1–4}$) and four VSD–pore coupling constants $D_{1–4}$ using the channel partition function:

$$Z = (1+J_1)(1+J_2)(1+J_3)(1+J_4) + L(1+J_1D_1)(1+J_2D_2)(1+J_3D_3)(1+J_4D_4).$$

The pore particle (L) derives its voltage dependence through a gating charge displacement Δq_L and a characteristic midpoint voltage V_L; for example, $L = \exp(\Delta q_L(V - V_L)/kT)$. Similar expressions applied to $J_{1–4}$ were used to describe intrinsic VSD activation. The four allosteric factors $D_{1–4}$ are related to VSD–pore interaction energies $W_{1–4}$ through $D_i = \exp(-W_i/kT)$.

The equilibrium curves $\langle k = l, j_{1–4} \rangle$ for the five gating particles are easily derived from the partition function through the relations $\langle k \rangle = \partial \ln Z / \partial \ln K$, which were used to fit the experimental conductance (G(V)) and fluorescence (F(V)) curves.

A kinetic model of channel activation that reduces to the thermodynamic model under equilibrium conditions was obtained by assigning two additional variables

for each particle transition: a frequency factor ν and a fractional position x of the transition barrier between resting and active states (Sigg, 2014). The forward and backward rate constants for the transition between a configuration i and any of the accessible configurations j after the activation of one of the five gating particles were expressed as

$$\alpha_{i\to j} = \nu_k \left(Z_j Z_i\right)^{xk}$$

and

$$\beta_{j\to i} = \nu_k \left(Z_i Z_j\right)^{1-xk},$$

where k refers to the transitioning particle and Z_i and Z_j are the configuration-specific contributions to the overall partition function Z (obtained by expanding the earlier expression of Z into its 32 terms).

The channel kinetics were solved by integrating $\overrightarrow{p}(t) = \overrightarrow{p}(0) \cdot \exp(Qt)$, which describes state probabilities of all states (p). Q is the standard rate matrix as described in Colquhoun and Hawkes (1981). The initial condition $p(0)$ for the holding potential was obtained from $\overrightarrow{p}$ $(t \to \infty)$. The time dependence of a quantity of interest A (ionic current or fluorescence) was obtained from

$$\langle A(t) \rangle = N \sum_i p_i(t)\, a_i,$$

where a_i is the value of the desired quantity at configuration i.

To find the set of parameters that best described the data, several approaches were used such as Marquadt–Levenberg, implemented in Berkeley Madonna, and Nedler–Mead, developed in Matlab, minimizing the error function "ssq" generated by the weighed sum of 10 error functions, five for steady-state voltage dependencies and five for time-dependent signals. Each individual error function corresponds to the sum of the squares of the difference between the experimental and simulated datasets normalized by n and the square of the maximum value.

To test for the uniqueness of the solution and estimating the 95% credible interval of each parameter, we used a Bayesian approach using Markov chain Monte Carlo (MCMC) sampling as in Hines et al. (2014), but instead of using likelihood ratio to test for high posterior probabilities, we used

$$a = \min\left[1, \exp\left(\frac{ssq_i - ssq_{i+1}}{T}\right)\right].$$

Then, transitions of the Markov chain were accepted with probability a, as described in Li (2012). To further constrain the solution space and take better advantage of the time-dependent data, we added a set of penalty functions as further explained in the supplementary figure legends.

Online supplemental material

Fig. S1 shows representative Ba^{2+} current traces from *Xenopus* oocytes expressing $Ca_V1.2$ channel complexes formed by α_{1C} + β_3 subunits. Fig. S2 shows histograms of posterior distributions of 14 parameters obtained from a 100,000-trial MCMC run. Fig. S3 shows histograms of posterior distributions of parameters x_i and n_i (i = L,1,2,3,4). Online supplemental material is available at http://www.jgp.org/cgi/content/full/jgp.201611586/DC1.

RESULTS

$\alpha_2\delta$-1 facilitates the voltage-dependent activation of human $Ca_V1.2$ channels

To understand the mechanism of $\alpha_2\delta$-1 subunits modulation of human $Ca_V1.2$ channels, we expressed in *Xenopus* oocytes $Ca_V1.2$ channels consisting of α_{1C} and β_3 subunits, in the presence or the absence of $\alpha_2\delta$-1 proteins. We voltage clamped the cells using the cut-open oocyte voltage clamp technique (Stefani and Bezanilla, 1998; Pantazis and Olcese, 2013) and recorded ionic currents (Fig. 2, A and B) using Ba^{2+} as the charge carrier to prevent calcium-dependent inactivation (Peterson et al., 1999; Qin et al., 1999). Because $Ca_V1.2$ channels lacking $\alpha_2\delta$-1 subunits activate slowly (Fig. 2 A), relatively longer depolarizations were necessary for ionic current to reach quasi–steady state (Fig. S1), a condition necessary to construct conductance versus voltage relationships (G(V)) from tail currents. We observed that $\alpha_2\delta$-1 coexpression strongly facilitated channel opening in human $Ca_V1.2$ channels by shifting the $Ca_V1.2$ half-activation potential (V_{half}) of the G(V) curves by ∼50 mV toward more hyperpolarized potentials (Fig. 2 C), in agreement with data previously obtained from the rabbit isoforms (Felix et al., 1997; Platano et al., 2000; Bourdin et al., 2015). G(V) curves obtained from channels expressed with the full complement of auxiliary subunits were well described by the sum of two Boltzmann functions with distinct voltage-dependent properties (V_{half1} = −4.02 ± 0.38 mV, z_1 = 3.46 ± 0.11 e^0, G_1 = 57.56 ± 4.82%, V_{half2} = 42.56 ± 1.87 mV, z_2 = 1.27 ± 0.04 e^0, G_2 = 42.44 ± 4.82%; n = 4; Fig. 2 C), alluding to a complex voltage-dependent activation mechanism with more than one voltage-dependent opening transitions; in contrast, G(V) curves for channels lacking $\alpha_2\delta$-1 were well accounted for by a single Boltzmann distribution (V_{half} = 68.01 ± 1.32 mV and z = 1.19 ± 0.01 e^0; n = 7), which is a tentative (yet tantalizing) indication that these channels gate in a two-state process. We further mechanistically evaluated this premise using an allosteric model of voltage-dependent Ca_V activation.

$\alpha_2\delta$-1 increases the rate of VSD I activation

Given the large difference (>50 mV) in the voltage dependence of $Ca_V1.2$ activation in the presence or ab-

sence of $\alpha_2\delta$-1 subunits (Fig. 2), we tested the hypothesis that $\alpha_2\delta$-1 association with α_{1C} induces a functional remodeling of one or more VSDs, altering their gating properties. We used the VCF technique (Mannuzzu et al., 1996; Cha and Bezanilla, 1997; Gandhi and Olcese, 2008) to track the molecular rearrangements of the individual VSDs of human $Ca_V1.2$ channels in the presence or absence of $\alpha_2\delta$-1. Briefly, this involves the introduction of a cysteine residue one at a time at a strategic and specific position extracellular to the S4 helix in each $Ca_V1.2$ VSD, as shown in our previous study (Pantazis et al., 2014). In voltage-gated ion channels, the S4 segment typically contains the positively charged amino acids effectively responsible for voltage sensing and undergoes structural rearrangements during depolarizations (Tombola et al., 2006; Bezanilla, 2008; Chanda and Bezanilla, 2008; Swartz, 2008; Catterall, 2010; Palovcak et al., 2014). $Ca_V1.2$ channels (α_{1C} + β_3 subunits) were expressed with or without $\alpha_2\delta$-1 subunits in *Xenopus* oocytes. After labeling of the cysteines with thiol-reactive fluorophores that are sensitive to the environment, we used VCF to simultaneously study the voltage-dependent activation of the pore (ionic current) and each of the four VSDs (fluorescence) in conducting $Ca_V1.2$ channels. The labeling positions and fluorophores used here were the same as in our previous work (Pantazis et al., 2014). The effect of $\alpha_2\delta$-1 subunits on the kinetics of VSD activation was quantified for 100-ms depolarizations to 20 mV (Table 1). The activation of VSD I was accelerated by approximately twofold by the $\alpha_2\delta$-1 subunit, increasing the fractional amplitude of the fast component of activation (Fig. 3 and Table 1). This result suggests that the acceleration of ionic current by the $\alpha_2\delta$-1 subunit (Fig. 2, A and B; Felix et al., 1997; Platano et al., 2000; Tuluc et al., 2007) may result from a faster VSD I, consistent with the findings of Nakai et al. (1994), who demonstrated a relevant role for VSD I in controlling $Ca_V1.2$ current kinetics by transferring $Ca_V1.1$ VSD I sequences into the corresponding location in $Ca_V1.2$. In contrast, the kinetics of VSDs II–IV were practically unaffected by $\alpha_2\delta$-1 (Fig. 3 and Table 1).

Table 1. **Effect of the $\alpha_2\delta$-1 subunit on $Ca_V1.2$ (α_{1C}/β_3) VSD activation kinetics (100-ms depolarizations to 20 mV)**

VSD	Parameter	No $\alpha_2\delta$	With $\alpha_2\delta$-1
VSD I	τ_1 (ms)	5.48 ± 1.57 (n = 4)	3.8 ± 0.37 (n = 3)
	α_1 (%)	47.2 ± 3.7	63.9 ± 7.7
	τ_2 (ms)	56.3 ± 7.9	29.6 ± 6.0
	τ_{avg} (ms)	31.4 ± 2.3	13.6 ± 3.7
VSD II	τ_1 (ms)	0.83 ± 0.32 (n = 3)	1.04 ± 0.39 (n = 3)
	α_1 (%)	43.1 ± 2.0	66.2 ± 8.6
	τ_2 (ms)	28.3 ± 12.5	30.7 ± 5.7
	τ_{avg} (ms)	16.5 ± 7.2	11.9 ± 3.6
VSD III	τ_1 (ms)	2.39 ± 0.44 (n = 6)	2.0 ± 0.17 (n = 4)
	α_1 (%)	91.8 ± 5.5	83.5 ± 9.7
	τ_2 (ms)	37.9 ± 7.9	32.0 ± 9.0
	τ_{avg} (ms)	4.6 ± 1.1	5.09 ± 0.98
VSD IV	τ_1 (ms)	21.5 ± 1.9 (n = 6)	16.5 ± 2.1 (n = 3)
	α_1 (%)	100	100
	τ_2 (ms)	NA	NA
	τ_{avg} (ms)	21.5 ± 1.9	16.5 ± 2.1

NA, not applicable.

$\alpha_2\delta$-1 facilitates the voltage-dependent activation of VSDs I, II, and III

To assess how the voltage dependence of the individual VSDs was affected by $\alpha_2\delta$-1 subunit association, we constructed activation curves (F(V)) from the corresponding fluorescence intensity at the end of 100-ms pulses

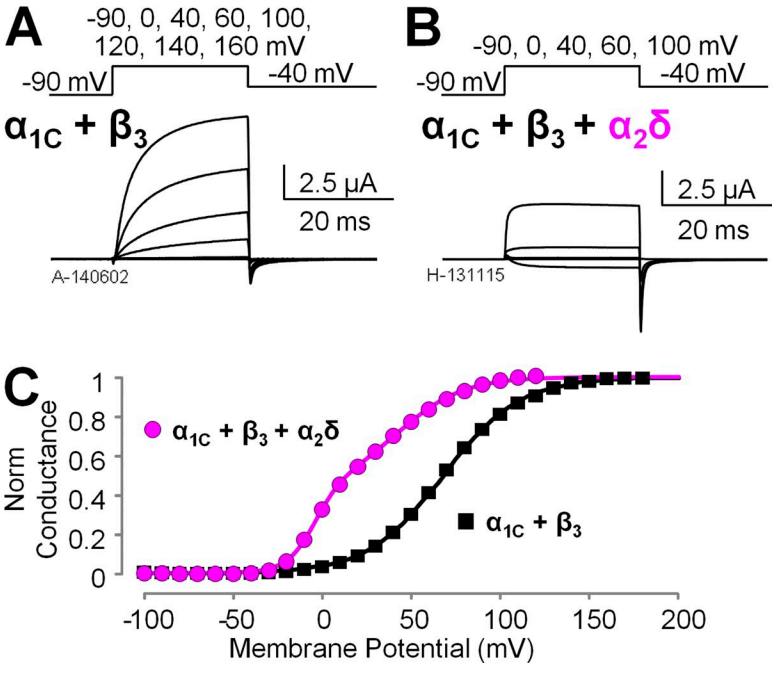

Figure 2. **The $\alpha_2\delta$-1 subunit facilitates $Ca_V1.2$ channel opening.** (A and B) Representative Ba^{2+} current traces from *Xenopus* oocytes expressing human $Ca_V1.2$ channel complexes with different subunit composition: α_{1C} + β_3 subunits (A) or α_{1C} + β_3 + $\alpha_2\delta$-1 subunits (B). The voltage protocol is reported above the current traces. (C) Mean conductance versus voltage (G(V)) relationships were constructed from tail currents as in B and Fig. S1 (mean ± SEM; error bars are within the symbols; n = 7 for α_{1C} + β_3 and n = 4 for α_{1C} + β_3 + $\alpha_2\delta$-1). The $\alpha_2\delta$-1 auxiliary subunit facilitates channel opening, as manifested by a hyperpolarizing shift of the conductance voltage dependence by ~50 mV.

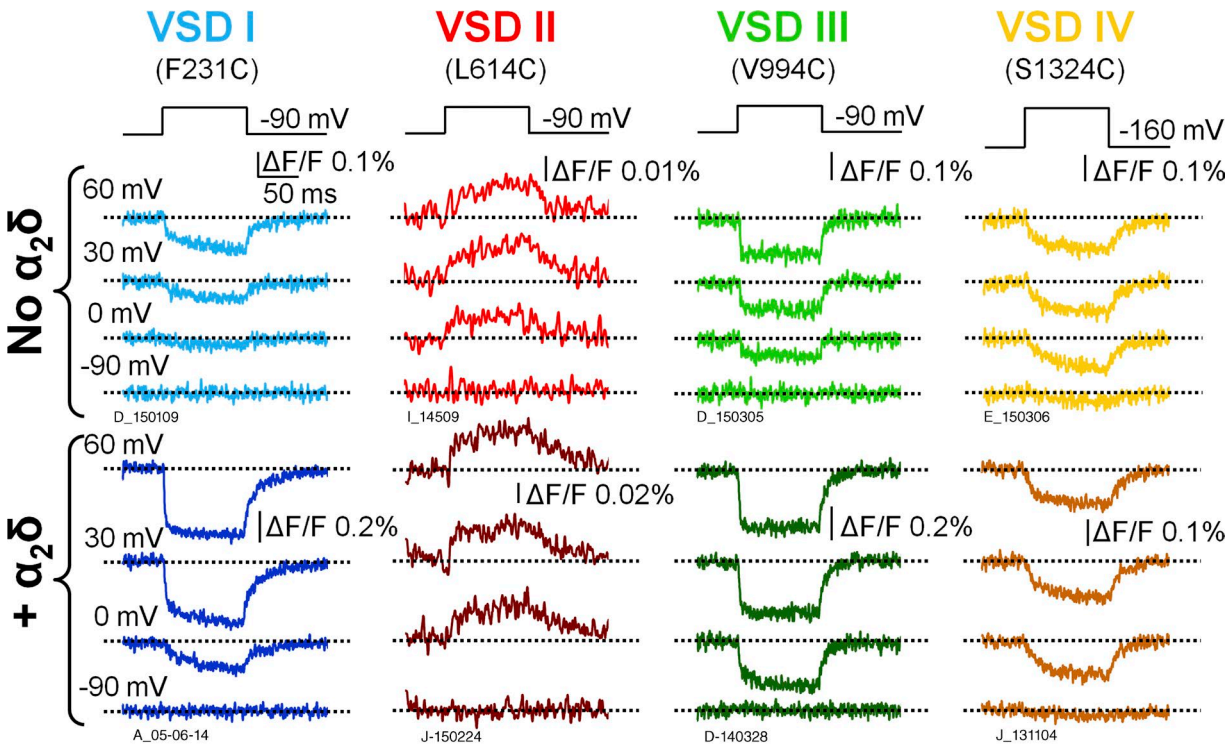

Figure 3. **Voltage-dependent rearrangements of the individual $Ca_V1.2$ VSDs in the presence and absence of the $\alpha_2\delta$ subunit.** Fluorescence traces reporting the structural rearrangements of each $Ca_V1.2$ VSD in the absence (top) or presence (bottom) of the $\alpha_2\delta$-1 subunit are shown. The channels were expressed in *Xenopus* oocytes and fluorescently labeled at extracellular S4 positions in VSD I (F231C), VSD II (L614C), VSD III (V994C), or VSD IV (S1324C). The voltage protocol is reported above the traces. The holding potential was –90 mV. Because VSD IV was partially activated at –90 mV (Fig. 4 D), oocytes expressing S1324C channels underwent a prepulse to –160 mV to allow VSD IV to return to its resting state before each depolarization.

over a wide range of membrane potentials (Fig. 4). The F(V) values of VSDs I–III were shifted to more negative potentials in the presence of the $\alpha_2\delta$-1 subunit, whereas VSD IV activation was unaffected (Fig. 4, A–D). Moreover, VSDs I–III exhibited a steeper slope of voltage-dependent activation: the effective charge q increased by approximately twofold (Fig. 4, A–C; and Table 2). Overall, in the absence of the $\alpha_2\delta$-1 subunit, the activation curves of the four VSDs were highly disparate, spread over a voltage range spanning ∼90 mV (Fig. 5 A and Table 2), while the variance of the V_{half} values was 1,300 mV^2. The association of $\alpha_2\delta$-1 subunit narrowed the range of membrane potentials at which VSDs activated (∼50 mV; Table 2, V_{half} variance: 520 mV^2) and shifted the G(V) such that VSD voltage dependence was closer to pore opening (Fig. 5 B). A separation of the half activation potential of VSD activation and channel opening can be interpreted as decreased coupling between VSD activation and pore gating (Sigg, 2014). Taken together, these results are consistent with the view that $\alpha_2\delta$-1 is required to increase the coupling between VSDs I–III and the $Ca_V1.2$ pore. In addition, because the effective charge q is the summed displacements of residue charges across the membrane potential profile, we cannot exclude that $\alpha_2\delta$-1 association also increases $Ca_V1.2$ voltage sensitivity by altering the shape of the profile (for example, making it steeper in the region of charge translation). To discriminate among these mechanisms (increased coupling, increased effective charge, or both), we modeled $Ca_V1.2$ activation with an allosteric model used previously (Pantazis et al., 2014).

$\alpha_2\delta$-1 facilitates $Ca_V1.2$ activation by increasing the energetic contribution of VSDs I–III to pore opening

We analyzed the VCF data with the 32-state allosteric model for $Ca_V1.2$ activation (Pantazis et al., 2014), consisting of five gating elements (one pore, four VSDs; Fig. 6 A) and therefore relevant to $Ca_V1.2$ architecture. Pore and VSDs can exist in two states: closed-open and resting-active, each undergoing voltage-dependent transitions. Thus, in this model, the pore as well as the VSDs are intrinsically voltage dependent (half-activation potential V and charge displacement q). The activation of one or more VSDs stabilizes the open state of the pore through energy coupling with magnitude W_i (i = 1–4).

Kinetic and quasi-equilibrium data from the pore (ionic currents) and each VSD (fluorescence) were simultaneously fitted in the absence of $\alpha_2\delta$-1 with no assumption or constraint. The model accurately accounts

Table 2. **Fitting parameters for the Boltzmann functions fitting the fluorescence data from each VSD (Fig. 4)**

VSD	Parameter	No $\alpha_2\delta$	With $\alpha_2\delta$–1
VSD I	q (e^0)	1.6 ± 0.1 (n = 5)	2.8 ± 0.1 (n = 5)
	V_{half} (mV)	36.5 ± 3.1	6.1 ± 1.3
VSD II	q (e^0)	1.2 ± 0.1 (n = 6)	2.7 ± 0.2 (n = 3)
	V_{half} (mV)	−6.7 ± 1.8	−30.8 ± 3.9
VSD III	q (e^0)	0.9 ± 0.1 (n = 6)	1.5 ± 0.09 (n = 5)
	V_{half} (mV)	0.9 ± 4.1	−22.0 ± 1.7
VSD IV	q (e^0)	0.9 ± 0.04 (n = 7)	1.1 ± 0.1 (n = 4)
	V_{half} (mV)	−51.4 ± 4	−48.5 ± 2.5

for the voltage- and time-dependent properties of channels composed of $\alpha_{1C} + \beta_3$ subunits (Fig. 6, B and C). The most salient feature of the fitted quantities is that the energetic contribution to pore opening (W) of each VSD is small (<1 kT or 25 meV). A comparison of W values with and without the $\alpha_2\delta$-1 subunit demonstrates a doubling of the energetic contribution to pore opening by VSDs I and III (W_1 and W_3) and an approximately threefold increase of W_2 in the presence of $\alpha_2\delta$-1, whereas the contribution of VSD IV (W_4) was practically unchanged (Table 3; parameters with $\alpha_2\delta$-1 are from Pantazis et al., 2014 and reported here for clarity). In addition to enhancing VSD I–III energetic contributions to pore opening, $\alpha_2\delta$-1 increased the charge displacement (q) of VSDs I and II by ∼140% and ∼200%, respectively (Table 3). In contrast, the intrinsic pore parameters q_L and V_L varied minimally with the addition of $\alpha_2\delta$-1 to the channel. Thus, $\alpha_2\delta$-1 modulates the $Ca_V1.2$ channel by exerting its effect on the VSDs (VSDs I–III) rather than on the pore.

The uniqueness of the solution and the 95% credible interval of each parameter were obtained with a Bayesian approach using MCMC sampling as in Hines et al. (2014). The results are reported in Figs. S2 and S3.

DISCUSSION

The α_1 subunit of voltage-gated Ca_V channels is a modular, pseudotetrameric protein consisting of a central pore domain coupled to four homologous but not identical VSDs. Several auxiliary subunits, including $\alpha_2\delta$ and β, associate with the α_1 subunit in a 1:1:1 ratio (Catterall, 2011; Wu et al., 2015) to regulate channel trafficking and biophysical properties (Fang and Colecraft, 2011; Dolphin, 2012; Neely and Hidalgo, 2014; Campiglio and Flucher, 2015). Using VCF to optically track the individual VSDs in a human $Ca_V1.2$ $\alpha_1 + \beta_3$ complex with and without the auxiliary $\alpha_2\delta$-1 subunits, we gained a mechanistic understanding of $\alpha_2\delta$-1–mediated facilitation of $Ca_V1.2$ activation. We found that $\alpha_2\delta$-1 alters the biophysical properties of three VSDs (I–III). The association of $\alpha_2\delta$-1 with α_{1C} increases the coupling of VSDs I–III to the channel pore, allowing the $Ca_V1.2$ channel to operate in the range of physiological membrane potentials found in excitable cells.

The physical nature of $\alpha_{1C}/\alpha_2\delta$-1 association

The association of $\alpha_2\delta$-1 with α_{1C} resulted in a substantial change in the intrinsic voltage-sensing properties of VSDs I–III (Fig. 4 and Table 3). This effect suggests either a direct physical or long-range allosteric interac-

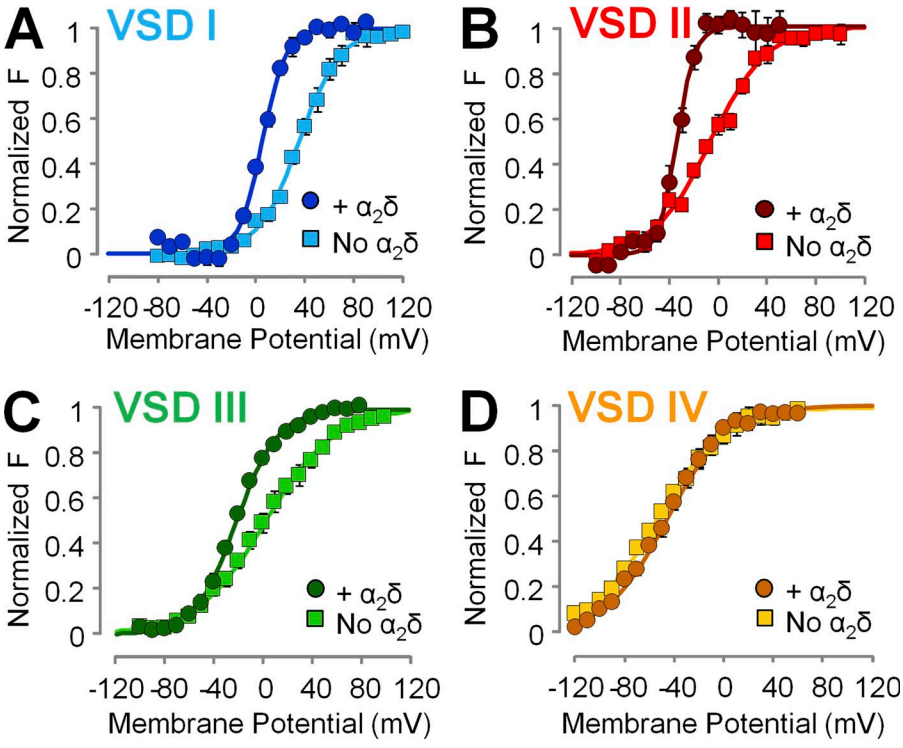

Figure 4. **The $\alpha_2\delta$-1 subunit facilitates the voltage-dependent activation of $Ca_V1.2$ VSDs I–III, whereas VSD IV is unperturbed.** (A–D) Mean voltage dependence of VSD activation constructed from experiments as in Fig. 3. The $\alpha_2\delta$-1 subunit facilitated the activation of VSDs I–III, as revealed by a more hyperpolarized voltage dependence of VSD activation, although to a different extent, whereas VSD IV was unaffected. Boltzmann fitting parameters are reported in Table 2.

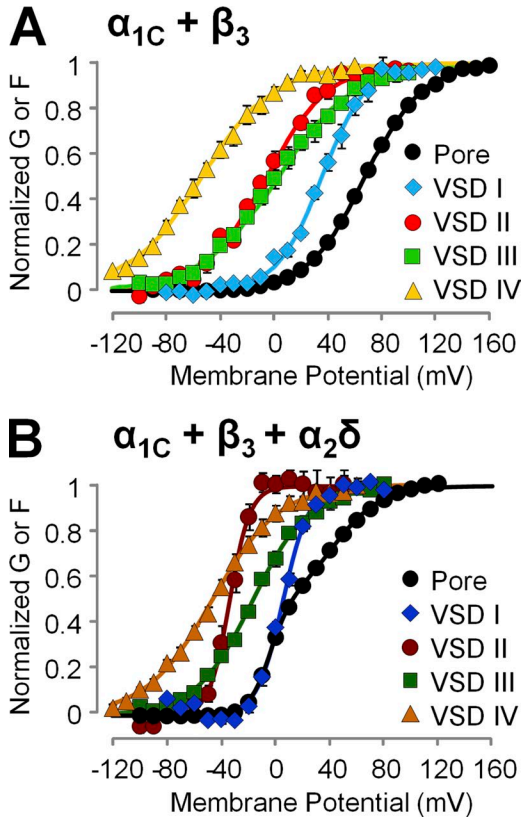

Figure 5. **The $\alpha_2\delta$-1 subunit remodels VSDs I–III.** (A and B) Mean normalized G(V) and F(V) data points from α_{1C} + β_3 (A) or α_{1C} + β_3 + $\alpha_2\delta$-1 (B) channels and the corresponding Boltzmann fits are shown superimposed (mean ± SEM). These results suggest that the facilitation of voltage-dependent pore activation by $\alpha_2\delta$-1 subunits is likely mediated by the remodeling of VSDs I–III.

tion of $\alpha_2\delta$-1 with these VSDs, causing their structural rearrangement. Our results are consistent with coimmunoprecipitation experiments showing that $\alpha_2\delta$ subunits bind to extracellular loops of repeat III and possibly to other extracellular loops of α_1 (Gurnett et al., 1997). On the other hand, VSD IV remained completely unaffected, suggesting that $\alpha_2\delta$-1 and VSD IV do not physically interact and consistent with the findings by Tuluc et al. (2009), who showed that the deletion of S3-S4 loop in VSD IV affects channel gating in $Ca_V1.1$ but not its modulation by $\alpha_2\delta$-1 subunits. The findings that three VSDs out of four are remodeled by $\alpha_2\delta$-1 is in agreement with a low-resolution structure of $Ca_V1.2$ channel complexes, which demonstrates that the $\alpha_2\delta$-1 subunit forms a cap that embraces ~3/4 of the extracellular surface of the α_{1C} subunit (Walsh et al., 2009a,b). Taking these data together, we propose that the $\alpha_2\delta$-1 encapsulates a part of α_{1C} that comprises VSDs I–III, whereas the exposed quarter of the α_{1C} subunit is VSD IV (Fig. 7). Finally, we favor a physical interaction between $\alpha_2\delta$-1 and VSDs I–III because of a recent cryo-electron microscopy (cryo-EM) structure of $Ca_V1.1$ channels showing that the $\alpha_2\delta$-1 subunit interacts with the extracellular loops of repeats I–III (Wu et al., 2015), suggesting a common $\alpha_1/\alpha_2\delta$ topology in $Ca_V1.1$ (α_{1S}) and $Ca_V1.2$ (α_{1C}) channels. However, contribution of long-range allosteric interactions cannot be ruled out.

$\alpha_2\delta$-1 association alters the intrinsic voltage-sensing properties of VSDs I–III

The hyperpolarizing shifts in the F(V) values of VSDs I–III (Fig. 4) indicates that the active state of these voltage sensors is favored in the presence of $\alpha_2\delta$-1 subunits. In VSD-gated channels, the activation of charge-bearing S4 segments is facilitated by the formation of salt bridges between positively charged S4 residues and negatively charged residues in adjacent VSD helices (Papazian et al., 1995; Wu et al., 2010; DeCaen et al., 2011; Tuluc et al., 2016). Association of the $\alpha_2\delta$-1 subunit may facilitate the formation of such bonds by physically remodeling the spatial organization of the transmembrane helices of VSDs, altering their relative positions. Interestingly, we found that the VSDs' sensitivity to changes in the membrane potential, i.e., the effective charge or slope of the F(V) curves (q), is almost equal among the four VSDs in the absence of the $\alpha_2\delta$-1 subunit ($q \approx 1\ e^0$), whereas q increases by approximately twofold for VSDs I–III in the presence of $\alpha_2\delta$-1. The effective charge q of a voltage-sensing residue is given by the product $z\delta$, where z is the valence number and δ is the electrical distance or fraction of membrane potential traversed by the residue. Because it is very unlikely that $\alpha_2\delta$-1 association adds voltage-sensing charges, the increased apparent charge observed for VSD I–III suggests that their charged S4 helices move across a greater electrical distance, through either a larger spatial translation (e.g., moving at a steeper angle) or more concentrated electric field lines. Indeed, in VSD-endowed proteins, the local electric field can be tremendously enhanced by the existence of aqueous crevices separated by hydrophobic gaskets comprised of aromatic residue side chains (Asamoah et al., 2003; Starace and Bezanilla, 2004; Ahern and Horn, 2005; Chanda et al., 2005; Long et al., 2007; Tao et al., 2010; Lacroix and Bezanilla, 2011).

The $\alpha_2\delta$-1 subunit enhances the coupling of VSDs I–III to the pore

Do the observed changes in VSD voltage-sensing properties account for the facilitation of $Ca_V1.2$ activation by $\alpha_2\delta$-1 subunit? To answer this question, we used our allosteric model for $Ca_V1.2$ channel activation, which predicts the time- and voltage-dependent properties of each VSD and the pore (Pantazis et al., 2014). This model successfully accounted for the effects of $\alpha_2\delta$-1 binding by both increasing the energetic contributions of VSDs I–III to pore opening and increasing the effective charges of VSDs I and II (Fig. 6 and Table 3). Specifically, in channels lacking the $\alpha_2\delta$-1 subunit, VSDs I–III

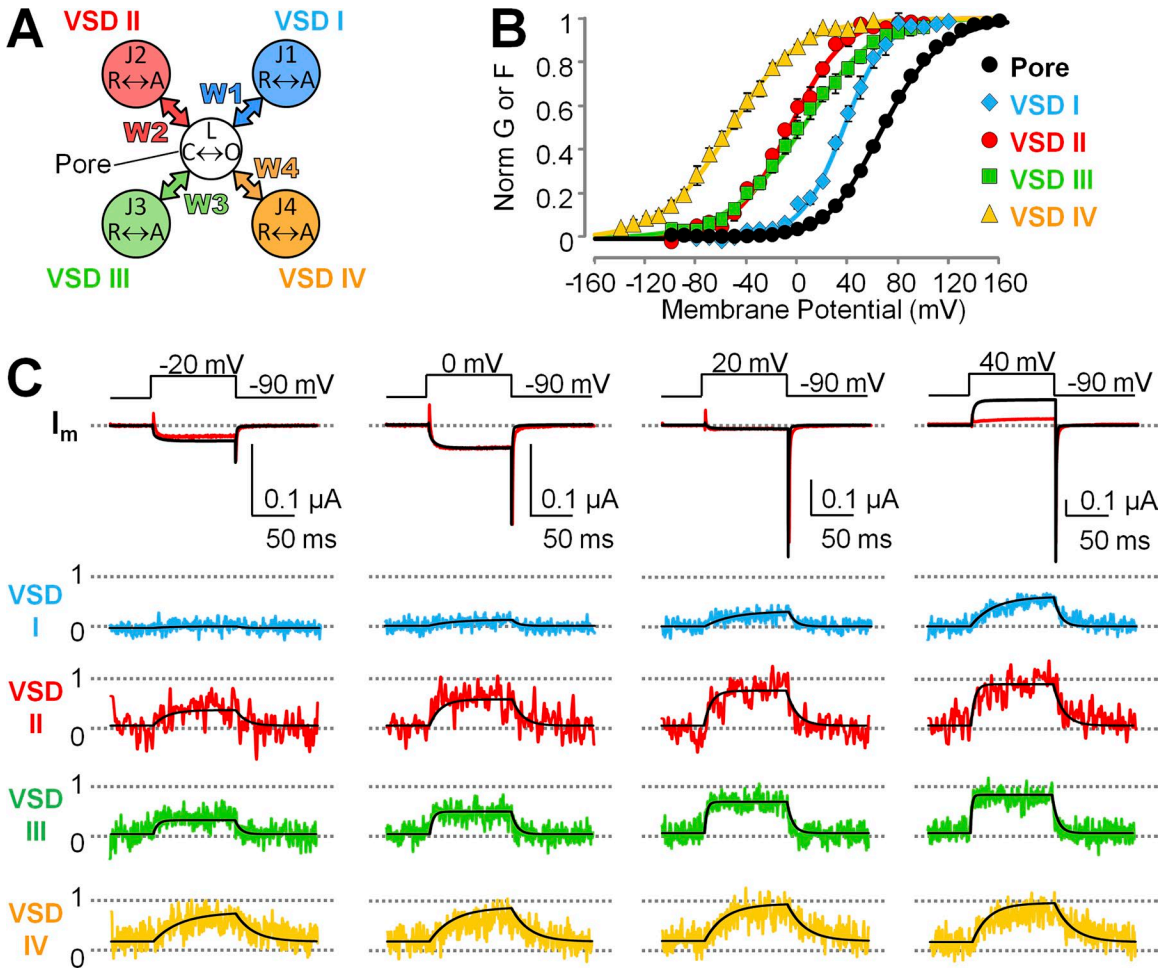

Figure 6. **An allosteric structure-based model of voltage-dependent $Ca_V1.2$ activation accounts for time- and voltage-dependent properties of $Ca_V1.2$ channels lacking the $\alpha_2\delta$-1 subunit.** (A) Scheme of the model used to simultaneously fit current and optically tracked conformational changes from each of the four $Ca_V1.2$ VSDs. Each VSD and the pore are modeled as two-state particles that can undergo resting↔active or closed↔open voltage-dependent transitions, respectively. Activation of a VSD allosterically stabilizes the open pore state by energy *W*. (B) Mean normalized G(V) and F(V) data points from α_{1C} + β_3 channels are shown superimposed with the model predictions (curves). (C) Ionic currents (top) and fluorescence traces from each VSD (normalized to VSD activation; bottom) from α_{1C} + β_3 channels. The simultaneous model fits are shown superimposed as black lines. Fitting parameters are reported in Table 3.

make a weak contribution to channel opening ($W > -20$ meV, equivalent to 0.8 kT or an allosteric factor of 2.2). The striking outcome of this study is that the energetic contribution of the activation of VSDs II and III to pore opening in channels lacking $\alpha_2\delta$ is greatly reduced. This is in contrast to channels containing $\alpha_2\delta$-1, where VSDs II and III contribute two to three times as much energy toward channel opening (~−95 meV, ~3.7 kT) or, in an alternative interpretation, their activation is obligatory for pore opening (Pantazis et al., 2014). The diminished VSD–pore conformational coupling in channels lacking $\alpha_2\delta$ is also supported by the good approximation of the G(V) by a Boltzmann distribution (Fig. 2 C), which implies a single voltage-dependent opening transition without significant input from VSDs. Our previous work on $\alpha_2\delta$-containing $Ca_V1.2$ channels revealed a surprising disparity in the VSD voltage dependencies, greater than that observed in related pseudotetrameric Na_V channels: VSD activations (V_{half} values) spanned 50 mV. The functional heterogeneity of the four VSDs was attributed to (a) the different amino acid composition of each VSD and (b) the structural asymmetry of the channel complex arising from its 1:1:1 $\alpha_1/\beta/\alpha_2\delta$ subunit stoichiometry. Interestingly, in this work, we found that increasing $Ca_V1.2$ structural symmetry (by excluding $\alpha_2\delta$-1 subunits) in fact made the VSD voltage dependencies even more disparate, spanning ~90 mV (Fig. 5). Our current model interpreted this finding as a result of direct modification of VSD voltage-sensing properties and reduced coupling of VSDs I–III to the pore by $\alpha_2\delta$-1. Another possible explanation is that $\alpha_2\delta$-1 acts as an allosteric center (in addition to the pore), increasing the coupling between voltage sensors. However, this possibility implies that $\alpha_2\delta$-1 also undergoes conformational changes,

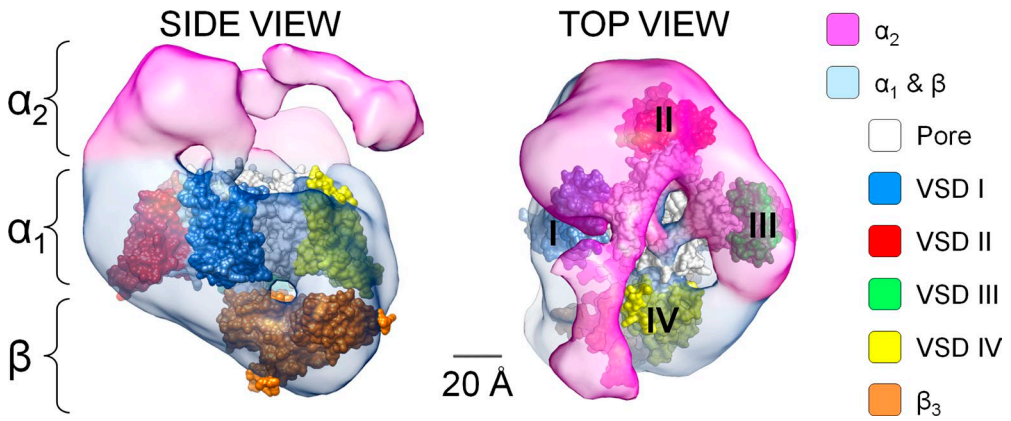

Figure 7. **The $\alpha_2\delta$ subunit covers ~3/4 of the $Ca_V1.2$ pore-forming subunit, excluding VSD IV.** Side and top views of the $Ca_V1.2$ ($\alpha_{1C}/\alpha_2/\beta$) channel volume (pink and light blue) modified from cryo-EM data from Walsh et al. (2009a) are shown. The atomic structures of Na_VAb (PDB accession no. 4EKW; Payandeh et al., 2012), with subunits arranged clockwise, and the atomic structure of AID-associated β_3 subunit (PDB accession no. 1VYT; Chen et al., 2004) were manually positioned in the cryo-EM volume. Because VSD IV is not perturbed by $\alpha_2\delta$-1, we propose that the resolved α_{1C} volume not covered by α_2 is occupied by VSD IV, whereas VSDs I–III are encompassed by the $\alpha_2\delta$-1 subunit, which alters their biophysical properties and, in the case of VSDs II and III, enhances their coupling to the channel pore.

for which there is yet no experimental evidence. Perhaps future studies could explore the possibility.

Conclusions

In summary, we have used VCF to optically track the molecular rearrangements of the individual VSDs of a human $Ca_V1.2$ channel in the presence or absence of $\alpha_2\delta$-1. VCF is now a well-established method to assess voltage-dependent conformational changes, allowing us to track the movement of individual VSDs and to resolve slow conformational changes (as those observed in VSD I) that are extremely difficult to capture by gating current measurements. In this work, we have not systematically recorded gating currents, as they could not reveal the individual contributions of each VSD to $Ca_V1.2$ activation. Perhaps the most important advantage of VCF is that all recordings could be performed in conducting channels, whereby ionic currents and VSD movements were sampled simultaneously, without the use of pore-blockers. We found that the $\alpha_2\delta$-1 auxiliary subunit significantly alters the voltage dependence of VSDs I–III, facilitating their activation, but not that of VSD IV. A 32-state allosteric model, consistent with the $Ca_V1.2$ molecular architecture, predicts the major kinetic and steady-state features of the experimental data, revealing that the association of $\alpha_2\delta$-1 with α_{1C} (in the presence of β_3) specifically increased the coupling energy of VSDs I–III to the pore, as well as effective gating charge in segments I and II. Without the enhanced gating properties brought about by $\alpha_2\delta$-1 association, $Ca_V1.2$ channels could not operate at physiological membrane potentials.

Table 3. **Fitting parameters for the model predictions in Fig. 6**

	Parameter	No $\alpha_2\delta$	With $\alpha_2\delta$-1[a]
Pore	q_L (e^0)	0.99	0.76
	V_L (mV)	103	140
	x_L	1.0	0.49
	ν_L (s^{-1})	1,356	670
VSD I	q_1 (e^0)	1.4	2.0
	V_1 (mV)	37	8.5
	x_1	0.72	0.89
	ν_1 (s^{-1})	17	110
VSD II	q_2 (e^0)	1.2	2.5
	V_2 (mV)	−6.9	−27
	x_2	0.78	0.99
	ν_2 (s^{-1})	35	44
VSD III	q_3 (e^0)	0.83	1.0
	V_3 (mV)	3.7	−11
	x_3	1.0	0.93
	ν_3 (s^{-1})	145	160
VSD IV	q_4 (e^0)	0.92	1.1
	V_4 (mV)	−54	−52
	x_4	0.35	0.55
	ν_4 (s^{-1})	16	11
Energetic interaction	W_1 (meV)	−8.0	−16
	W_2 (meV)	−16	−50
	W_3 (meV)	−19	−45
	W_4 (meV)	4.1	−0.87

[a]Parameters in this column are from Pantazis et al., 2014.

ACKNOWLEDGMENTS

We are grateful to Ashraf Kitmitto for sharing the cryo-EM volumes of Ca_V $\alpha_{1C}/\alpha_2\delta$ (Walsh et al., 2009a). The human $\alpha_{1C\text{-}77}$ clone was a gift from Nicolaj Soldatov. We thank the members of the Olcese laboratory for insightful discussion and Jing Gao for the weekly preparation of the *Xenopus* oocytes.

This work was supported by the National Institutes of Health (NIH)/National Heart, Lung, and Blood Institute grant P01HL078931 to J.N. Weiss and R. Olcese; NIH/National Institute of General Medical Sciences grant R01GM110276 to R. Ol-

cese; American Heart Association Scientist Development grant 14SDG20300018 to A. Pantazis and postdoctoral fellowship 16POST27250284 to N. Savalli; and Chilean government grants FONDECYT 1161672 and ACT1104 to A. Neely. The Centro Interdisciplinario de Neurociencia de Valparaíso is a Millennium Institute supported by the Millennium Scientific Initiative of the Chilean Ministry of Economy.

The authors declare no competing financial interests.

Eduardo Rios served as editor.

Submitted: 17 February 2016
Accepted: 30 June 2016

REFERENCES

Ahern, C.A., and R. Horn. 2005. Focused electric field across the voltage sensor of potassium channels. *Neuron.* 48:25–29. http://dx.doi.org/10.1016/j.neuron.2005.08.020

Asamoah, O.K., J.P. Wuskell, L.M. Loew, and F. Bezanilla. 2003. A fluorometric approach to local electric field measurements in a voltage-gated ion channel. *Neuron.* 37:85–98. http://dx.doi.org/10.1016/S0896-6273(02)01126-1

Bangalore, R., G. Mehrke, K. Gingrich, F. Hofmann, and R.S. Kass. 1996. Influence of L-type Ca channel alpha 2/delta-subunit on ionic and gating current in transiently transfected HEK 293 cells. *Am. J. Physiol.* 270:H1521–H1528.

Barclay, J., N. Balaguero, M. Mione, S.L. Ackerman, V.A. Letts, J. Brodbeck, C. Canti, A. Meir, K.M. Page, K. Kusumi, et al. 2001. Ducky mouse phenotype of epilepsy and ataxia is associated with mutations in the Cacna2d2 gene and decreased calcium channel current in cerebellar Purkinje cells. *J. Neurosci.* 21:6095–6104.

Barish, M.E. 1983. A transient calcium-dependent chloride current in the immature *Xenopus* oocyte. *J. Physiol.* 342:309–325. http://dx.doi.org/10.1113/jphysiol.1983.sp014852

Ben-Johny, M., and D.T. Yue. 2014. Calmodulin regulation (calmodulation) of voltage-gated calcium channels. *J. Gen. Physiol.* 143:679–692. http://dx.doi.org/10.1085/jgp.201311153

Bezanilla, F. 2008. How membrane proteins sense voltage. *Nat. Rev. Mol. Cell Biol.* 9:323–332. http://dx.doi.org/10.1038/nrm2376

Bourdin, B., B. Shakeri, M.P. Tétreault, R. Sauvé, S. Lesage, and L. Parent. 2015. Functional characterization of CaVα2δ mutations associated with sudden cardiac death. *J. Biol. Chem.* 290:2854–2869. http://dx.doi.org/10.1074/jbc.M114.597930

Burashnikov, E., R. Pfeiffer, H. Barajas-Martinez, E. Delpón, D. Hu, M. Desai, M. Borggrefe, M. Häissaguerre, R. Kanter, G.D. Pollevick, et al. 2010. Mutations in the cardiac L-type calcium channel associated with inherited J-wave syndromes and sudden cardiac death. *Heart Rhythm.* 7:1872–1882. http://dx.doi.org/10.1016/j.hrthm.2010.08.026

Calderón-Rivera, A., A. Andrade, O. Hernández-Hernández, R. González-Ramírez, A. Sandoval, M. Rivera, J.C. Gomora, and R. Felix. 2012. Identification of a disulfide bridge essential for structure and function of the voltage-gated Ca(2+) channel α(2)δ-1 auxiliary subunit. *Cell Calcium.* 51:22–30. http://dx.doi.org/10.1016/j.ceca.2011.10.002

Campiglio, M., and B.E. Flucher. 2015. The role of auxiliary subunits for the functional diversity of voltage-gated calcium channels. *J. Cell. Physiol.* 230:2019–2031. http://dx.doi.org/10.1002/jcp.24998

Cassidy, J.S., L. Ferron, I. Kadurin, W.S. Pratt, and A.C. Dolphin. 2014. Functional exofacially tagged N-type calcium channels elucidate the interaction with auxiliary $\alpha_2\delta$-1 subunits. *Proc. Natl. Acad. Sci. USA.* 111:8979–8984. http://dx.doi.org/10.1073/pnas.1403731111

Catterall, W.A. 2010. Ion channel voltage sensors: Structure, function, and pathophysiology. *Neuron.* 67:915–928. http://dx.doi.org/10.1016/j.neuron.2010.08.021

Catterall, W.A. 2011. Voltage-gated calcium channels. *Cold Spring Harb. Perspect. Biol.* 3:a003947. http://dx.doi.org/10.1101/cshperspect.a003947

Cha, A., and F. Bezanilla. 1997. Characterizing voltage-dependent conformational changes in the Shaker K+ channel with fluorescence. *Neuron.* 19:1127–1140. http://dx.doi.org/10.1016/S0896-6273(00)80403-1

Cha, A., P.C. Ruben, A.L. George Jr., E. Fujimoto, and F. Bezanilla. 1999. Voltage sensors in domains III and IV, but not I and II, are immobilized by Na+ channel fast inactivation. *Neuron.* 22:73–87. http://dx.doi.org/10.1016/S0896-6273(00)80680-7

Chanda, B., and F. Bezanilla. 2008. A common pathway for charge transport through voltage-sensing domains. *Neuron.* 57:345–351. http://dx.doi.org/10.1016/j.neuron.2008.01.015

Chanda, B., O.K. Asamoah, R. Blunck, B. Roux, and F. Bezanilla. 2005. Gating charge displacement in voltage-gated ion channels involves limited transmembrane movement. *Nature.* 436:852–856. http://dx.doi.org/10.1038/nature03888

Chen, Y.H., M.H. Li, Y. Zhang, L.L. He, Y. Yamada, A. Fitzmaurice, Y. Shen, H. Zhang, L. Tong, and J. Yang. 2004. Structural basis of the alpha1-beta subunit interaction of voltage-gated Ca2+ channels. *Nature.* 429:675–680. http://dx.doi.org/10.1038/nature02641

Claydon, T.W., and D. Fedida. 2007. Voltage clamp fluorimetry studies of mammalian voltage-gated K(+) channel gating. *Biochem. Soc. Trans.* 35:1080–1082. http://dx.doi.org/10.1042/BST0351080

Colquhoun, D., and A.G. Hawkes. 1981. On the stochastic properties of single ion channels. *Proc. R. Soc. Lond. B Biol. Sci.* 211:205–235. http://dx.doi.org/10.1098/rspb.1981.0003

Dahan, D.S., M.I. Dibas, E.J. Petersson, V.C. Auyeung, B. Chanda, F. Bezanilla, D.A. Dougherty, and H.A. Lester. 2004. A fluorophore attached to nicotinic acetylcholine receptor βM2 detects productive binding of agonist to the αδ site. *Proc. Natl. Acad. Sci. USA.* 101:10195–10200. http://dx.doi.org/10.1073/pnas.0301885101

Davies, A., I. Kadurin, A. Alvarez-Laviada, L. Douglas, M. Nieto-Rostro, C.S. Bauer, W.S. Pratt, and A.C. Dolphin. 2010. The α2δ subunits of voltage-gated calcium channels form GPI-anchored proteins, a posttranslational modification essential for function. *Proc. Natl. Acad. Sci. USA.* 107:1654–1659. http://dx.doi.org/10.1073/pnas.0908735107

DeCaen, P.G., V. Yarov-Yarovoy, T. Scheuer, and W.A. Catterall. 2011. Gating charge interactions with the S1 segment during activation of a Na+ channel voltage sensor. *Proc. Natl. Acad. Sci. USA.* 108:18825–18830. http://dx.doi.org/10.1073/pnas.1116449108

Dolphin, A.C. 2012. Calcium channel auxiliary α2δ and β subunits: Trafficking and one step beyond. *Nat. Rev. Neurosci.* 13:542–555. http://dx.doi.org/10.1038/nrn3317

Dolphin, A.C. 2013. The α2δ subunits of voltage-gated calcium channels. *Biochim. Biophys. Acta.* 1828:1541–1549. http://dx.doi.org/10.1016/j.bbamem.2012.11.019

Eroglu, C., N.J. Allen, M.W. Susman, N.A. O'Rourke, C.Y. Park, E. Ozkan, C. Chakraborty, S.B. Mulinyawe, D.S. Annis, A.D. Huberman, et al. 2009. Gabapentin receptor alpha2delta-1 is a neuronal thrombospondin receptor responsible for excitatory CNS synaptogenesis. *Cell.* 139:380–392. http://dx.doi.org/10.1016/j.cell.2009.09.025

Fang, K., and H.M. Colecraft. 2011. Mechanism of auxiliary β-subunit-mediated membrane targeting of L-type (Ca(V)1.2) channels. *J. Physiol.* 589:4437–4455. http://dx.doi.org/10.1113/jphysiol.2011.214247

Felix, R., C.A. Gurnett, M. De Waard, and K.P. Campbell. 1997. Dissection of functional domains of the voltage-dependent Ca2+ channel alpha2delta subunit. *J. Neurosci.* 17:6884–6891.

Field, M.J., P.J. Cox, E. Stott, H. Melrose, J. Offord, T.Z. Su, S. Bramwell, L. Corradini, S. England, J. Winks, et al. 2006. Identification of the α2-δ-1 subunit of voltage-dependent calcium channels as a molecular target for pain mediating the analgesic actions of pregabalin. *Proc. Natl. Acad. Sci. USA.* 103:17537–17542. http://dx.doi.org/10.1073/pnas.0409066103

Findeisen, F., and D.L. Minor Jr. 2010. Progress in the structural understanding of voltage-gated calcium channel (CaV) function and modulation. *Channels (Austin).* 4:459–474. http://dx.doi.org/10.4161/chan.4.6.12867

Fuller-Bicer, G.A., G. Varadi, S.E. Koch, M. Ishii, I. Bodi, N. Kadeer, J.N. Muth, G. Mikala, N.N. Petrashevskaya, M.A. Jordan, et al. 2009. Targeted disruption of the voltage-dependent calcium channel α_2/δ-1-subunit. *Am. J. Physiol. Heart Circ. Physiol.* 297:H117–H124. http://dx.doi.org/10.1152/ajpheart.00122.2009

Gandhi, C.S., and R. Olcese. 2008. The voltage-clamp fluorometry technique. *Methods Mol. Biol.* 491:213–231. http://dx.doi.org/10.1007/978-1-59745-526-8_17

Ghezzi, C., H. Murer, and I.C. Forster. 2009. Substrate interactions of the electroneutral Na+-coupled inorganic phosphate cotransporter (NaPi-IIc). *J. Physiol.* 587:4293–4307. http://dx.doi.org/10.1113/jphysiol.2009.175596

Gurnett, C.A., R. Felix, and K.P. Campbell. 1997. Extracellular interaction of the voltage-dependent Ca2+ channel alpha2delta and alpha1 subunits. *J. Biol. Chem.* 272:18508–18512. http://dx.doi.org/10.1074/jbc.272.29.18508

Hendrich, J., A.T. Van Minh, F. Heblich, M. Nieto-Rostro, K. Watschinger, J. Striessnig, J. Wratten, A. Davies, and A.C. Dolphin. 2008. Pharmacological disruption of calcium channel trafficking by the α2δ ligand gabapentin. *Proc. Natl. Acad. Sci. USA.* 105:3628–3633. http://dx.doi.org/10.1073/pnas.0708930105

Hines, K.E., T.R. Middendorf, and R.W. Aldrich. 2014. Determination of parameter identifiability in nonlinear biophysical models: A Bayesian approach. *J. Gen. Physiol.* 143:401–416. http://dx.doi.org/10.1085/jgp.201311116

Kohout, S.C., M.H. Ulbrich, S.C. Bell, and E.Y. Isacoff. 2008. Subunit organization and functional transitions in Ci-VSP. *Nat. Struct. Mol. Biol.* 15:106–108. http://dx.doi.org/10.1038/nsmb1320

Kurshan, P.T., A. Oztan, and T.L. Schwarz. 2009. Presynaptic alpha2delta-3 is required for synaptic morphogenesis independent of its Ca2+-channel functions. *Nat. Neurosci.* 12:1415–1423. http://dx.doi.org/10.1038/nn.2417

Lacroix, J.J., and F. Bezanilla. 2011. Control of a final gating charge transition by a hydrophobic residue in the S2 segment of a K+ channel voltage sensor. *Proc. Natl. Acad. Sci. USA.* 108:6444–6449. http://dx.doi.org/10.1073/pnas.1103397108

Larsson, H.P., A.V. Tzingounis, H.P. Koch, and M.P. Kavanaugh. 2004. Fluorometric measurements of conformational changes in glutamate transporters. *Proc. Natl. Acad. Sci. USA.* 101:3951–3956. http://dx.doi.org/10.1073/pnas.0306737101

Li, Y. 2012. MOMCMC: An efficient Monte Carlo method for multi-objective sampling over real parameter space. *Comput. Math. Appl.* 64:3542–3556. http://dx.doi.org/10.1016/j.camwa.2012.09.003

Li, C.Y., X.L. Zhang, E.A. Matthews, K.W. Li, A. Kurwa, A. Boroujerdi, J. Gross, M.S. Gold, A.H. Dickenson, G. Feng, and Z.D. Luo. 2006. Calcium channel alpha2delta1 subunit mediates spinal hyperexcitability in pain modulation. *Pain.* 125:20–34. http://dx.doi.org/10.1016/j.pain.2006.04.022

Long, S.B., X. Tao, E.B. Campbell, and R. MacKinnon. 2007. Atomic structure of a voltage-dependent K+ channel in a lipid membrane-like environment. *Nature.* 450:376–382. http://dx.doi.org/10.1038/nature06265

Lörinczi, É., Y. Bhargava, S.F. Marino, A. Taly, K. Kaczmarek-Hájek, A. Barrantes-Freer, S. Dutertre, T. Grutter, J. Rettinger, and A. Nicke. 2012. Involvement of the cysteine-rich head domain in activation and desensitization of the P2X1 receptor. *Proc. Natl. Acad. Sci. USA.* 109:11396–11401. http://dx.doi.org/10.1073/pnas.1118759109

Mannuzzu, L.M., M.M. Moronne, and E.Y. Isacoff. 1996. Direct physical measure of conformational rearrangement underlying potassium channel gating. *Science.* 271:213–216. http://dx.doi.org/10.1126/science.271.5246.213

Meinild, A.K., B.A. Hirayama, E.M. Wright, and D.D. Loo. 2002. Fluorescence studies of ligand-induced conformational changes of the Na(+)/glucose cotransporter. *Biochemistry.* 41:1250–1258. http://dx.doi.org/10.1021/bi011661r

Nakai, J., B.A. Adams, K. Imoto, and K.G. Beam. 1994. Critical roles of the S3 segment and S3-S4 linker of repeat I in activation of L-type calcium channels. *Proc. Natl. Acad. Sci. USA.* 91:1014–1018. http://dx.doi.org/10.1073/pnas.91.3.1014

Neely, A., and P. Hidalgo. 2014. Structure-function of proteins interacting with the α_1 pore-forming subunit of high-voltage-activated calcium channels. *Front. Physiol.* 5:209. http://dx.doi.org/10.3389/fphys.2014.00209

Neely, A., R. Olcese, X. Wei, L. Birnbaumer, and E. Stefani. 1994. Ca(2+)-dependent inactivation of a cloned cardiac Ca2+ channel alpha 1 subunit (alpha 1C) expressed in Xenopus oocytes. *Biophys. J.* 66:1895–1903. http://dx.doi.org/10.1016/S0006-3495(94)80983-X

Neely, G.G., A. Hess, M. Costigan, A.C. Keene, S. Goulas, M. Langeslag, R.S. Griffin, I. Belfer, F. Dai, S.B. Smith, et al. 2010. A genome-wide *Drosophila* screen for heat nociception identifies α2δ3 as an evolutionarily conserved pain gene. *Cell.* 143:628–638. http://dx.doi.org/10.1016/j.cell.2010.09.047

Osteen, J.D., C. Gonzalez, K.J. Sampson, V. Iyer, S. Rebolledo, H.P. Larsson, and R.S. Kass. 2010. KCNE1 alters the voltage sensor movements necessary to open the KCNQ1 channel gate. *Proc. Natl. Acad. Sci. USA.* 107:22710–22715. http://dx.doi.org/10.1073/pnas.1016300108

Palovcak, E., L. Delemotte, M.L. Klein, and V. Carnevale. 2014. Evolutionary imprint of activation: The design principles of VSDs. *J. Gen. Physiol.* 143:145–156. http://dx.doi.org/10.1085/jgp.201311103

Pantazis, A., and R. Olcese. 2013. Cut-open oocyte voltage clamp technique. *In* Encyclopedia of Biophysics. G.C.K. Roberts, editor. Springer, Berlin, Heidelberg. 406–413. http://dx.doi.org/10.1007/978-3-642-16712-6_371

Pantazis, A., N. Savalli, D. Sigg, A. Neely, and R. Olcese. 2014. Functional heterogeneity of the four voltage sensors of a human L-type calcium channel. *Proc. Natl. Acad. Sci. USA.* 111:18381–18386. http://dx.doi.org/10.1073/pnas.1411127112

Papazian, D.M., X.M. Shao, S.A. Seoh, A.F. Mock, Y. Huang, and D.H. Wainstock. 1995. Electrostatic interactions of S4 voltage sensor in Shaker K+ channel. *Neuron.* 14:1293–1301. http://dx.doi.org/10.1016/0896-6273(95)90276-7

Payandeh, J., T.M. Gamal El-Din, T. Scheuer, N. Zheng, and W.A. Catterall. 2012. Crystal structure of a voltage-gated sodium channel in two potentially inactivated states. *Nature.* 486:135–139.

Peterson, B.Z., C.D. DeMaria, J.P. Adelman, and D.T. Yue. 1999. Calmodulin is the Ca^{2+} sensor for Ca^{2+}-dependent inactivation of L-type calcium channels. *Neuron.* 22:549–558. http://dx.doi.org/10.1016/S0896-6273(00)80709-6

Platano, D., N. Qin, F. Noceti, L. Birnbaumer, E. Stefani, and R. Olcese. 2000. Expression of the alpha(2)delta subunit interferes with prepulse facilitation in cardiac L-type calcium channels. *Biophys. J.* 78:2959–2972. http://dx.doi.org/10.1016/S0006-3495(00)76835-4

Qin, N., R. Olcese, M. Bransby, T. Lin, and L. Birnbaumer. 1999. Ca2+-induced inhibition of the cardiac Ca2+ channel depends on calmodulin. *Proc. Natl. Acad. Sci. USA*. 96:2435–2438. http://dx.doi.org/10.1073/pnas.96.5.2435

Ruscic, K.J., F. Miceli, C.A. Villalba-Galea, H. Dai, Y. Mishina, F. Bezanilla, and S.A. Goldstein. 2013. IKs channels open slowly because KCNE1 accessory subunits slow the movement of S4 voltage sensors in KCNQ1 pore-forming subunits. *Proc. Natl. Acad. Sci. USA*. 110:E559–E566. http://dx.doi.org/10.1073/pnas.1222616110

Savalli, N., A. Kondratiev, L. Toro, and R. Olcese. 2006. Voltage-dependent conformational changes in human Ca(2+)- and voltage-activated K(+) channel, revealed by voltage-clamp fluorometry. *Proc. Natl. Acad. Sci. USA*. 103:12619–12624. http://dx.doi.org/10.1073/pnas.0601176103

Savalli, N., A. Kondratiev, S.B. de Quintana, L. Toro, and R. Olcese. 2007. Modes of operation of the BKCa channel beta2 subunit. *J. Gen. Physiol.* 130:117–131. http://dx.doi.org/10.1085/jgp.200709803

Sigg, D. 2014. Modeling ion channels: Past, present, and future. *J. Gen. Physiol.* 144:7–26. http://dx.doi.org/10.1085/jgp.201311130

Smith, P.L., and G. Yellen. 2002. Fast and slow voltage sensor movements in HERG potassium channels. *J. Gen. Physiol.* 119:275–293. http://dx.doi.org/10.1085/jgp.20028534

Soldatov, N.M. 1992. Molecular diversity of L-type Ca2+ channel transcripts in human fibroblasts. *Proc. Natl. Acad. Sci. USA*. 89:4628–4632. http://dx.doi.org/10.1073/pnas.89.10.4628

Starace, D.M., and F. Bezanilla. 2004. A proton pore in a potassium channel voltage sensor reveals a focused electric field. *Nature*. 427:548–553. http://dx.doi.org/10.1038/nature02270

Stefani, E., and F. Bezanilla. 1998. Cut-open oocyte voltage-clamp technique. *Methods Enzymol.* 293:300–318. http://dx.doi.org/10.1016/S0076-6879(98)93020-8

Swartz, K.J. 2008. Sensing voltage across lipid membranes. *Nature*. 456:891–897. http://dx.doi.org/10.1038/nature07620

Talwar, S., and J.W. Lynch. 2015. Investigating ion channel conformational changes using voltage clamp fluorometry. *Neuropharmacology*. 98:3–12. http://dx.doi.org/10.1016/j.neuropharm.2015.03.018

Tao, X., A. Lee, W. Limapichat, D.A. Dougherty, and R. MacKinnon. 2010. A gating charge transfer center in voltage sensors. *Science*. 328:67–73. http://dx.doi.org/10.1126/science.1185954

Templin, C., J.R. Ghadri, J.S. Rougier, A. Baumer, V. Kaplan, M. Albesa, H. Sticht, A. Rauch, C. Puleo, D. Hu, et al. 2011. Identification of a novel loss-of-function calcium channel gene mutation in short QT syndrome (SQTS6). *Eur. Heart J.* 32:1077–1088. http://dx.doi.org/10.1093/eurheartj/ehr076

Tombola, F., M.M. Pathak, and E.Y. Isacoff. 2006. How does voltage open an ion channel? *Annu. Rev. Cell Dev. Biol.* 22:23–52. http://dx.doi.org/10.1146/annurev.cellbio.21.020404.145837

Tombola, F., M.H. Ulbrich, S.C. Kohout, and E.Y. Isacoff. 2010. The opening of the two pores of the Hv1 voltage-gated proton channel is tuned by cooperativity. *Nat. Struct. Mol. Biol.* 17:44–50. http://dx.doi.org/10.1038/nsmb.1738

Tuluc, P., G. Kern, G.J. Obermair, and B.E. Flucher. 2007. Computer modeling of siRNA knockdown effects indicates an essential role of the Ca^{2+} channel $\alpha_2\delta$-1 subunit in cardiac excitation-contraction coupling. *Proc. Natl. Acad. Sci. USA*. 104:11091–11096. http://dx.doi.org/10.1073/pnas.0700577104

Tuluc, P., N. Molenda, B. Schlick, G.J. Obermair, B.E. Flucher, and K. Jurkat-Rott. 2009. A CaV1.1 Ca2+ channel splice variant with high conductance and voltage-sensitivity alters EC coupling in developing skeletal muscle. *Biophys. J.* 96:35–44. http://dx.doi.org/10.1016/j.bpj.2008.09.027

Tuluc, P., V. Yarov-Yarovoy, B. Benedetti, and B.E. Flucher. 2016. Molecular interactions in the voltage sensor controlling gating properties of CaV calcium channels. *Structure*. 24:261–271. http://dx.doi.org/10.1016/j.str.2015.11.011

Uchitel, O.D., M.N. Di Guilmi, F.J. Urbano, and C. Gonzalez-Inchauspe. 2010. Acute modulation of calcium currents and synaptic transmission by gabapentinoids. *Channels (Austin)*. 4:490–496. http://dx.doi.org/10.4161/chan.4.6.12864

Vergult, S., A. Dheedene, A. Meurs, F. Faes, B. Isidor, S. Janssens, A. Gautier, C. Le Caignec, and B. Menten. 2015. Genomic aberrations of the CACNA2D1 gene in three patients with epilepsy and intellectual disability. *Eur. J. Hum. Genet.* 23:628–632. http://dx.doi.org/10.1038/ejhg.2014.141

Walsh, C.P., A. Davies, A.J. Butcher, A.C. Dolphin, and A. Kitmitto. 2009a. Three-dimensional structure of CaV3.1: Comparison with the cardiac L-type voltage-gated calcium channel monomer architecture. *J. Biol. Chem.* 284:22310–22321. http://dx.doi.org/10.1074/jbc.M109.017152

Walsh, C.P., A. Davies, M. Nieto-Rostro, A.C. Dolphin, and A. Kitmitto. 2009b. Labelling of the 3D structure of the cardiac L-type voltage-gated calcium channel. *Channels (Austin)*. 3:387–392. http://dx.doi.org/10.4161/chan.3.6.10225

Wu, D., K. Delaloye, M.A. Zaydman, A. Nekouzadeh, Y. Rudy, and J. Cui. 2010. State-dependent electrostatic interactions of S4 arginines with E1 in S2 during Kv7.1 activation. *J. Gen. Physiol.* 135:595–606. http://dx.doi.org/10.1085/jgp.201010408

Wu, J., Z. Yan, Z. Li, C. Yan, S. Lu, M. Dong, and N. Yan. 2015. Structure of the voltage-gated calcium channel Cav1.1 complex. *Science*. 350:aad2395. http://dx.doi.org/10.1126/science.aad2395

Wycisk, K.A., C. Zeitz, S. Feil, M. Wittmer, U. Forster, J. Neidhardt, B. Wissinger, E. Zrenner, R. Wilke, S. Kohl, and W. Berger. 2006. Mutation in the auxiliary calcium-channel subunit CACNA2D4 causes autosomal recessive cone dystrophy. *Am. J. Hum. Genet.* 79:973–977. http://dx.doi.org/10.1086/508944

Zamponi, G.W., J. Striessnig, A. Koschak, and A.C. Dolphin. 2015. The physiology, pathology, and pharmacology of voltage-gated calcium channels and their future therapeutic potential. *Pharmacol. Rev.* 67:821–870. http://dx.doi.org/10.1124/pr.114.009654

Zhu, W., Z. Varga, and J.R. Silva. 2016. Molecular motions that shape the cardiac action potential: Insights from voltage clamp fluorometry. *Prog. Biophys. Mol. Biol.* 120:3–17. http://dx.doi.org/10.1016/j.pbiomolbio.2015.12.003